THE JOURNAL OF PHYSICAL CHEMISTRY C

Article

pubs.acs.org/JPCC

Interfacial Charge Carrier Dynamics of the Three-Component In_2O_3–TiO_2–Pt Heterojunction System

Yu-Chih Chen, Ying-Chih Pu, and Yung-Jung Hsu*

Department of Materials Science and Engineering, National Chiao Tung University, Hsinchu, Taiwan 30010, Republic of China

ABSTRACT: The interfacial charge carrier dynamics of the three-component semiconductor–semiconductor–metal heterojunction system were investigated and presented for the first time. The samples were prepared by selectively depositing Pt nanoparticles on the TiO_2 surface of In_2O_3-decorated TiO_2 nanobelts (In_2O_3–TiO_2 nanobelts (NBs)) using the typical photodeposition method. For In_2O_3–TiO_2 NBs, because of the difference in band structures between In_2O_3 and TiO_2, the photoexcited electrons of In_2O_3 nanocrystals would preferentially transfer to TiO_2 NBs to cause charge carrier separation. With the introduction of Pt on TiO_2 surface, a fluent electron transfer from In_2O_3, through TiO_2, and eventually to Pt was achieved, giving rise to the increasingly pronounced charge separation property for the as-prepared In_2O_3–TiO_2–Pt NBs. The remarkable charge separation of the samples was revealed with the corresponding photocurrent measurements. Time-resolved photoluminescence spectra were measured to quantitatively analyze the electron transfer event between In_2O_3 and TiO_2 for In_2O_3–TiO_2 NBs and its dependence on Pt deposition. Upon the deposition of Pt, In_2O_3–TiO_2 NBs showed an increased apparent electron-scavenging rate constant, fundamentally consistent with the result of their performance evaluation in photocatalysis. The current study provides a new paradigm for designing highly efficient three-component nanoheterojunction photocatalysts which can effectively produce chemical energy from absorbing light.

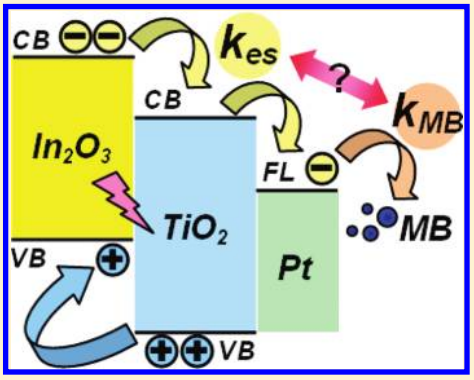

INTRODUCTION

Modulation of charge carrier dynamics for semiconductors is important to the development of light-energy conversion systems.[1] One effective way to affect charge transfer of semiconductor and hence boost carrier collection is to couple it with another semiconductor having appropriate band structure.[2,3] Because of the relative band alignment of the two constituent semiconductors, spatial separation of electrons and holes following photoexcitation may be promoted, bringing these binary composites highly desirable properties for photoconversion applications. By suitably controlling the systematic conditions for the binary semiconductor composites, a significant enhancement in the photoconversion efficiency can be further achieved. For example, a 2-fold increase in the incident-photon-to-current efficiency was observed for CdSe-decorated TiO_2 nanotubes once the size of CdSe was decreased from 3.7 to 2.3 nm.[4] This enhancement is due to the more energetic excited state of smaller CdSe, which ensures the faster electron injection from excited CdSe into TiO_2 and thus the more efficient collection of electrons. Besides, through adjusting the solution alkalinity to tune the band edge of TiO_2, a one-order of magnitude difference in electron injection rate was revealed in the CdSe-TiO_2 composite system.[5] This result demonstrates the possibility of improving the photoconversion efficiency for binary semiconductor composites by means of solution pH.

In addition to the binary system, three-component heterojunction composites have also been extensively investigated in recent years.[6,7] With the introduction of additional constituent, the photoexcited electrons and holes of binary hybrid semiconductors can be separated in a more effective manner, rendering them much better performance in relevant photoconversion processes. For instance, through depositing Pt on the TiO_2 surface of the CdS-TiO_2 composite, a fluent electron transfer from CdS, through TiO_2, and eventually to Pt was achieved, while the photogenerated holes remained at CdS domain to cause charge carrier separation.[7] Because of the spatial separation of electrons and holes into two well-spaced regions, CdS–TiO_2–Pt heterojunction exhibited improved photocurrent generation and higher photocatalytic activity as compared to its binary counterparts of CdS–Pt, TiO_2–Pt, as well as CdS–TiO_2. Another three-component hybrid example that has been intensively examined is the Z-scheme heterogeneous system, in which metal is included at the interface of binary semiconductor composite acting as the electron-transfer mediator to enhance the oxidizing and reducing powers for photocatalysis.[8] Till now, miscellaneous kinds of three-component semiconductor composites have been proposed and fabricated to further the advancement of photoconversion technology.[6−9] There are however very few studies in the literature regarding the charge carrier dynamics of three-component heterojunction system, and their correlation with the resultant photoconversion efficiency is rarely reported. Therefore, a quantitative study on this topic is essential and

Received: October 19, 2011
Revised: December 29, 2011
Published: January 9, 2012

   dx.doi.org/10.1021/jp210033y | *J. Phys. Chem. C* 2012, 116, 2967–2975

crucial to both the fundamental understanding and the practical applications for the ternary hybrid system.

In this work, we presented a prototype semiconductor−semiconductor−metal heterojunction system by selectively depositing Pt nanoparticles on the TiO_2 surface of In_2O_3-decorated TiO_2 nanobelts (denoted as In_2O_3−TiO_2 NBs). For In_2O_3−TiO_2 NBs, TiO_2 can serve as an effective electron scavenger for the surface-attached In_2O_3 due to its lower conduction band potential (the bottom of conduction band, −0.29 V vs NHE) than that of In_2O_3 (−0.62 V vs NHE).[10] As a consequence, the photoexcited electrons of In_2O_3 nanocrystals would preferentially transfer to TiO_2 NBs, leaving photogenerated holes at In_2O_3 domains to achieve charge separation. Because of the electron-charged feature of TiO_2 under light illumination, Pt nanoparticles can be further deposited on TiO_2 surface of In_2O_3−TiO_2 NBs using the typical photodeposition method, which resulted in the formation of three-component In_2O_3−TiO_2−Pt heterojunction NBs. Time-resolved photoluminescence (PL) measurements were conducted to explore the interfacial charge carrier dynamics for the as-prepared In_2O_3−TiO_2−Pt NBs. By probing the emission lifetime of an indicator dye, the electron transfer event between In_2O_3 and TiO_2 for In_2O_3−TiO_2 NBs and its dependence on Pt deposition were quantitatively analyzed. With the introduction of Pt on TiO_2 surface, In_2O_3−TiO_2 NBs showed an increased apparent electron-scavenging rate constant, attributable to the deposited Pt that can mediate the interfacial charge transfer of NBs to promote the overall charge separation efficiency. The charge carrier transfer in In_2O_3−TiO_2−Pt NBs under light illumination was further characterized with a photocatalytic process. It was found that In_2O_3−TiO_2−Pt NBs surpassed pristine TiO_2 NBs, pure In_2O_3 nanocrystals, and In_2O_3−TiO_2 NBs in photocatalytic activity, presumably due to the more pronounced charge separation property of In_2O_3−TiO_2−Pt heterojunction system. As compared to the commercial P-25 TiO_2 powder, the as-synthesized In_2O_3−TiO_2−Pt NBs exhibited superior photocatalytic performance under UV illumination, demonstrating their potential as an active photocatalyst in relevant redox reactions. In addition, the result of performance evaluation under natural sunlight shows that the present In_2O_3−TiO_2−Pt NBs may practically harvest energy from sunlight.

EXPERIMENTAL SECTION

Chemicals. All chemicals were analytic-grade reagents and used without further purification.

Preparation of Anatase TiO_2 NBs. The detailed synthetic approach and relevant characterizations of anatase TiO_2 NBs used here can be found in our previous work.[11] Briefly, Degussa P-25 TiO_2 powder (1.0 g), absolute ethanol (10 mL), and NaOH aqueous solution (10 mL, 10 M) were mixed and allowed for hydrothermal reaction at 200 °C for 24 h. The resultant white slurry was immersed in HCl solution (0.1M) for 24 h, producing hydrogen titanate ($H_2Ti_3O_7$) NBs. $H_2Ti_3O_7$ NBs of a fixed amount were then calcinated at 700 °C in air for 4 h to obtain anatase TiO_2 NBs.[12]

Preparation of In_2O_3−TiO_2 NBs. The decoration of In_2O_3 on TiO_2 NBs was carried out in a precipitation-annealing process. In the typical procedure, $InCl_3$ powder (221.2 mg, 1.0 mmol) was dissolved in deionized water (5 mL) containing a trace amount of NH_4OH (500 μL, 1.0 M), followed by the addition of TiO_2 NBs (40.0 mg, 0.5 mmol). After stirring at room temperature for 12 h, pale yellow suspending solids were produced in the reaction solution. The resultant precipitate was washed, collected, and further annealed at 700 °C in air for 2 h to produce In_2O_3-decorated TiO_2 NBs. For comparison purposes, pure In_2O_3 nanocrystals were also prepared using the same procedure without the addition of NBs.

Deposition of Pt on TiO_2 Surface of In_2O_3−TiO_2 NBs. To achieve Pt deposition on TiO_2 surface, In_2O_3−TiO_2 NBs (5.0 mg) were first dispersed in absolute ethanol (20 mL) in a quartz tube. H_2PtCl_6 solution (50 μL) of a desirable concentration was then added in the quartz tube. Upon a fixed period of UV irradiation (λ = 365 nm, 8 W) under vigorous stirring, the suspending solid was collected by centrifugation at 10,000 rpm for 10 min and washed with distilled water and ethanol to remove remaining ions. In this work, various concentrations of H_2PtCl_6 (5, 25, 50 mM) added in the reaction solution were employed to deposit Pt with different amounts. From scanning electron microscopy and energy dispersive X-ray spectrometry (SEM-EDS) analysis, the content of Pt deposited on In_2O_3−TiO_2 NBs was determined to be 1.0, 5.0, and 10.0 wt % for the employment of H_2PtCl_6 of 5, 25, and 50 mM, respectively. The product thus obtained was, respectively, denoted as In_2O_3−TiO_2−Pt-1, In_2O_3−TiO_2−Pt-5, and In_2O_3−TiO_2−Pt-10 NBs.

Photocurrent Measurement. Photocurrent measurements for the NB products were conducted in a photoelectrochemical system under white light irradiation (xenon lamp, 500 W) without applying an external bias. Note that white light irradiation which matches well natural sunlight in spectral distribution was applied in order to demonstrate the applicability of NBs in solar energy conversion. Spin-coated film of the sample on fluorine-doped tin oxide (FTO) substrate was used as the photoanode in the three-electrode cell which consisted of Pt counter electrode, Ag/AgCl reference electrode, and 0.01 M NaOH redox couple.[13]

PL Lifetime Measurement. Time-resolved PL spectra were measured using a home-built single photon counting system. GaN diode laser (λ = 375 nm) with the pulse duration of 50 ps was used as the excitation source. The signals collected at the excitonic emission of rhodamine B (denoted as RhB, λ_{em} = 581 nm) were dispersed with a grating spectrometer, detected by a high-speed photomultiplier tube, and then correlated using a single photon counting card. Here, RhB (1.0×10^{-6} M) was used as an indicator dye to monitor the interfacial charge transfer for In_2O_3−TiO_2−Pt NBs. Upon laser excitation, the photoexcited electrons of RhB were injected into In_2O_3 due to the higher lowest-unoccupied molecular orbital (LUMO) potential of RhB (−1.10 V vs NHE)[14] than the conduction band potential of In_2O_3 (−0.62 V vs NHE), which led to a significant quenching on the fluorescence of RhB. By comparing the emission decay profiles between RhB and In_2O_3-containing RhB (denoted as RhB/In_2O_3), the electron transfer from RhB to In_2O_3 can be quantitatively deduced. Further spectral comparison among RhB/In_2O_3, RhB/TiO_2, and RhB/In_2O_3−TiO_2 samples may reveal the electron transfer event between In_2O_3 and TiO_2. It should be noted that the PL emissions of In_2O_3 and TiO_2 were mainly located at wavelength less than 500 nm (including excitonic band-to-band and trap-state related emissions), with which the emission decay of RhB at 581 nm was not interfered and its variation with the presence of In_2O_3, TiO_2, In_2O_3−TiO_2, Pt, and In_2O_3−TiO_2−Pt can be precisely interpreted. The emission decay data were analyzed and fitted with an appropriate exponential model in which the decay component (τ_i), the preexponential factor (A_i), and the

dx.doi.org/10.1021/jp210033y | J. Phys. Chem. C 2012, 116, 2967−2975

Table 1. Kinetic Analysis of Emission Decay for RhB in the Presence of Different Samples

entry (I)	A_1	τ_1 (ns)	A_2	τ_2 (ns)	$\langle\tau\rangle$ (ns)	k_{et} (s^{-1})
RhB	10731.0	1.61			1.61	
RhB/TiO_2	9775.5	1.56			1.56	0.20×10 (RhB → TiO_2)[a]
RhB/Pt-1 (Pt = 1.0 wt %)	11213.0	1.59			1.59	0.08×10^8 (RhB → Pt-1)[a]
RhB/Pt-5 (Pt = 5.0 wt %)	10926.0	1.58			1.58	0.12×10^8 (RhB → Pt-5)[a]
RhB/Pt-10 (Pt = 10.0 wt %)	10751.0	1.55			1.55	0.24×10^8 (RhB → Pt-10)[a]
RhB/In_2O_3	1759.8	1.57	5012.8	0.20	1.21	2.05×10^8 (RhB → In_2O_3)[a]
RhB/In_2O_3–TiO_2	2026.8	1.50	8715.2	0.18	1.05	1.06×10^8 (In_2O_3 → TiO_2)[b]
RhB/In_2O_3–TiO_2–Pt-1 (Pt = 1.0 wt %)	1449.9	1.40	9385.2	0.17	0.86	2.03×10^8 (TiO_2 → Pt-1)[c]
entry (II)	A_1	τ_1 (ns)	A_2	τ_2 (ns)	$\langle\tau\rangle$ (ns)	k_{es} (s^{-1})
RhB/In_2O_3	1759.8	1.57	5012.8	0.20	1.21	
RhB/In_2O_3–TiO_2	2026.8	1.50	8715.2	0.18	1.05	1.06×10^8 (In_2O_3 → TiO_2)[b]
RhB/In_2O_3–TiO_2–Pt-1 (Pt = 1.0 wt %)	1449.9	1.40	9385.2	0.17	0.86	3.09×10^8 (In_2O_3 → TiO_2–Pt-1)[d]
RhB/In_2O_3–TiO_2–Pt-5 (Pt = 5.0 wt %)	975.2	1.29	9670.0	0.15	0.68	6.12×10^8 (In_2O_3 → TiO_2–Pt-5)[d]
RhB/In_2O_3–TiO_2–Pt-10 (Pt = 10.0 wt %)	1362.3	1.35	8610.0	0.16	0.80	3.80×10^8 (In_2O_3 → TiO_2–Pt-10)[d]

[a]The value was calculated by the expression

$$k_{et}(\mathrm{RhB} \rightarrow \mathrm{A}) = \frac{1}{\langle\tau\rangle}(\mathrm{RhB/A}) - \frac{1}{\langle\tau\rangle}(\mathrm{RhB})$$

where *A* represents TiO_2, Pt-1, Pt-5, Pt-10, or In_2O_3.

[b]The value was calculated by the expression

$$k_{et}(\mathrm{In_2O_3} \rightarrow \mathrm{TiO_2}) = \frac{1}{\langle\tau\rangle}(\mathrm{RhB/In_2O_3 - TiO_2}) - \frac{1}{\langle\tau\rangle}(\mathrm{RhB/In_2O_3}) - k_{et}(\mathrm{RhB} \rightarrow \mathrm{TiO_2})$$

[c]The value was calculated by the expression

$$k_{et}(\mathrm{TiO_2} \rightarrow \mathrm{Pt}) = \frac{1}{\langle\tau\rangle}(\mathrm{RhB/In_2O_3 - TiO_2 - Pt}) - \frac{1}{\langle\tau\rangle}(\mathrm{RhB/In_2O_3 - TiO_2}) - k_{et}(\mathrm{RhB} \rightarrow \mathrm{Pt})$$

[d]The value was calculated by the expression

$$k_{es}(\mathrm{A} \rightarrow \mathrm{B - C}) = \frac{1}{\langle\tau\rangle}(\mathrm{RhB/A - B - C}) - \frac{1}{\langle\tau\rangle}(\mathrm{RhB/A}) - k_{et}(\mathrm{RhB} \rightarrow \mathrm{B}) - k_{et}(\mathrm{RhB} \rightarrow \mathrm{C})$$

where *A* represents In_2O_3, *B* symbolizes TiO_2, and *C* stands for Pt-1, Pt-5, or Pt-10.

intensity-average lifetime ($\langle\tau\rangle$) were derived. For biexponential kinetics, the decay of PL intensity, $I(t)$, was analyzed by the equation $I(t) = A_1e^{-t/\tau_1} + A_2e^{-t/\tau_2}$ which generates two lifetime values, τ_1 and τ_2, and the corresponding amplitudes, A_1 and A_2.[15] The intensity-average lifetime, $\langle\tau\rangle$, was then determined using the following expression

$$\langle\tau\rangle = \frac{A_1{\tau_1}^2 + A_2{\tau_2}^2}{A_1\tau_1 + A_2\tau_2}$$

All the fitting results were summarized in Table 1.

Photocatalytic Activity Measurement. The photocatalytic activity of In_2O_3–TiO_2–Pt NBs was evaluated by the photodegradation of methylene blue (denoted as MB) under UV illumination. A quartz tube with a capacity of 30 mL was used as the photoreactor vessel. The optical system used for photocatalytic reaction consisted of UV lamp (8 W, λ = 365 nm) with a light intensity of 3.5 mW/cm^2. During the photocatalytic process, the photoreactor vessel was placed in a chamber equipped with eight concentrically encircling UV lamps, which ensured the spatially uniform illumination for MB solution in the vessel. All the photocatalysis experiments were performed at room temperature. Seven kinds of photocatalysts including pristine TiO_2 NBs, pure In_2O_3 nanocrystals, In_2O_3–TiO_2 NBs, three In_2O_3–TiO_2–Pt NB samples (In_2O_3–TiO_2–Pt-1, In_2O_3–TiO_2–Pt-5, In_2O_3–TiO_2–Pt-10), and Degussa P-25 TiO_2 powder were used and compared in the photodegradation of MB. Note that ethanol was used as the sacrificial hole scavenger for photocatalysts to facilitate the further utilization of photoexcited electrons.[11] Typically, a fixed amount of photocatalyst (5.0 mg) was added into MB ethanolic solution (20 mL, 1.0×10^{-5} M) in the photoreactor vessel. Prior to irradiation, the suspension was deaerated and stirred in the dark for 30 min to reach the adsorption equilibrium of MB with photocatalyst. At certain time intervals of irradiation, 1.5 mL of the reaction solution was withdrawn and centrifuged to remove photocatalyst particles. The filtrates were analyzed with a UV–visible spectrophotometer to measure the concentration

dx.doi.org/10.1021/jp210033y | J. Phys. Chem. C 2012, 116, 2967–2975

variation of MB through recording the corresponding absorbance of the characteristic peak at 665 nm. Since the photocatalysis experiments were conducted under a steady stirring condition, the concentration change of MB solution resulting from its reduced volume upon each of the sampling operations was quite insignificant. Furthermore, photodegradation of MB (1.0×10^{-5} M) under natural sunlight by using In_2O_3–TiO_2–Pt-5 (5.0 mg) as photocatalyst was also tested.

Characterizations. The morphology and dimensions of the products were examined with a field-emission scanning electron microscope (SEM, JEOL, JSM-6500F) and a high-resolution transmission electron microscope (HRTEM, JEOL, JEM-3000) operated at 300 kV. The crystallographic structure of the samples was investigated with X-ray diffraction (XRD, MAC Science, MXP18). The elemental analysis of individual NB was conducted with EDS, the accessory of SEM (JSM-6500F) and TEM (JEM-3000). Photocurrent signals were recorded with a Keithley 2400 semiconductor analyzer. For steady-state PL spectroscopy, a Hitachi F-4500 equipped with a xenon lamp (150 W) was used, and the emission spectra were collected with a scan speed of 1200 nm/min. UV–visible absorption spectra were obtained using a Hitachi U-3900H spectrophotometer at room temperature.

RESULTS AND DISCUSSION

Figure 1 represents the structural investigations of TiO_2 NBs after they were treated with $InCl_3$ in the precipitation-annealing process. SEM and TEM observations show that a large quantity of nanocrystals with the size of 20–50 nm were present on NB surfaces. The XRD pattern of Figure 1b reveals the existence of anatase TiO_2 along with body-centered cubic (bcc) In_2O_3 in the product, indicating that the surface-attached nanocrystals were composed of In_2O_3, while the NB support was the first-added TiO_2. Such nanocrystal-decorated NB feature of In_2O_3–TiO_2 was further confirmed by the TEM-EDS analysis shown in Figure 2d. Because of the difference in band structures between In_2O_3 and TiO_2, the photoexcited electrons of In_2O_3 nanocrystals would preferentially transfer to TiO_2 NBs to cause charge separation. This electron-charged characteristic of TiO_2 for In_2O_3–TiO_2 NBs upon light irradiation can be utilized to selectively deposit Pt on TiO_2 surface by using the typical photodeposition method. Since Pt photodeposition employing UV irradiation of H_2PtCl_6 solution is a chemical reduction process,[16] the electron-charged TiO_2 surface of In_2O_3–TiO_2 NBs may provide active sites for $PtCl_6^{2-}$ reduction and therefore direct the exclusive deposition of Pt on TiO_2. Parts a–c of Figure 2 display the morphology of In_2O_3–TiO_2 NBs after reacting with H_2PtCl_6 in the photodeposition process. Evidently, nanoparticles with quite small size (2–3 nm) were deposited on NB surfaces only. The corresponding TEM-EDS analysis in Figure 2d confirms the composition of these nanoparticles as Pt. More importantly, as increasing the concentration of H_2PtCl_6 employed, the amount of Pt nanoparticles deposited on TiO_2 surface of In_2O_3–TiO_2 NBs increased accordingly. With this outcome, we were able to study the quantitative effect of Pt deposition on the interfacial charge transfer of In_2O_3–TiO_2 NBs.

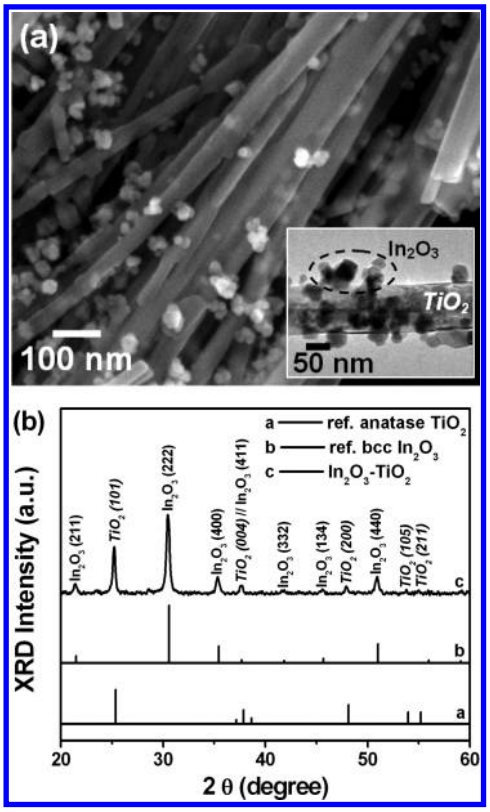

Figure 1. (a) SEM image and (b) XRD pattern for In_2O_3–TiO_2 NBs. Inset in (a) shows the corresponding TEM image. In (b), the patterns of reference anatase TiO_2 (JCPDS 89–4921) and bcc In_2O_3 (JCPDS 89–4595) were also included for comparison.

In this work, an indicator dye of RhB was used to monitor the charge carrier dynamics for the NB products. Note that employing RhB as a probe molecule to characterize the interfacial charge transfer of semiconductors is well-documented in literature.[17] Particularly, the variation of fluorescence intensity and lifetime at 581 nm is informative. Figure 3a shows the steady-state PL spectra of RhB under different experimental conditions. An obvious depression in the PL emission of RhB was first noticed when pure In_2O_3 nanocrystals of a given amount were dispersed in RhB (sample was denoted as RhB/In_2O_3). This depression became more pronounced as In_2O_3–TiO_2 NBs with commensurate amount were introduced (sample was denoted as RhB/In_2O_3–TiO_2). It should be mentioned that when being in contact with In_2O_3 nanocrystals or In_2O_3–TiO_2 NBs, RhB itself did not undergo photocatalysis to get decomposed during the short time period of PL measurement (within 20 s). The as-observed PL depression of RhB in RhB/In_2O_3 and in RhB/In_2O_3–TiO_2 samples was thus mainly attributed to the occurrence of charge separation and the prevalence of carrier transfer upon light irradiation. Note that In_2O_3 can serve as an effective electron scavenger for RhB due to its lower conduction band potential (−0.62 V vs NHE) than the LUMO potential of RhB (−1.10 V vs NHE). As a consequence, the photoexcited free electrons of RhB would preferentially transfer to In_2O_3, leading to the depletion of free electrons for RhB and the subsequent suppression of its fluorescence emission. When In_2O_3 was present along with TiO_2, the photoexcited electrons of RhB may further transfer to TiO_2 through the In_2O_3/TiO_2 interface by virtue of the much lower conduction band potential of TiO_2 (−0.29 V vs NHE). This phenomenon caused a higher extent of free electron depletion for RhB, which is responsible for the more pronounced PL depression of RhB observed for RhB/In_2O_3–TiO_2 sample. Further deposition of Pt on TiO_2 surface of In_2O_3–TiO_2 NBs led to a much more significant quenching in

dx.doi.org/10.1021/jp210033y | J. Phys. Chem. C 2012, 116, 2967–2975

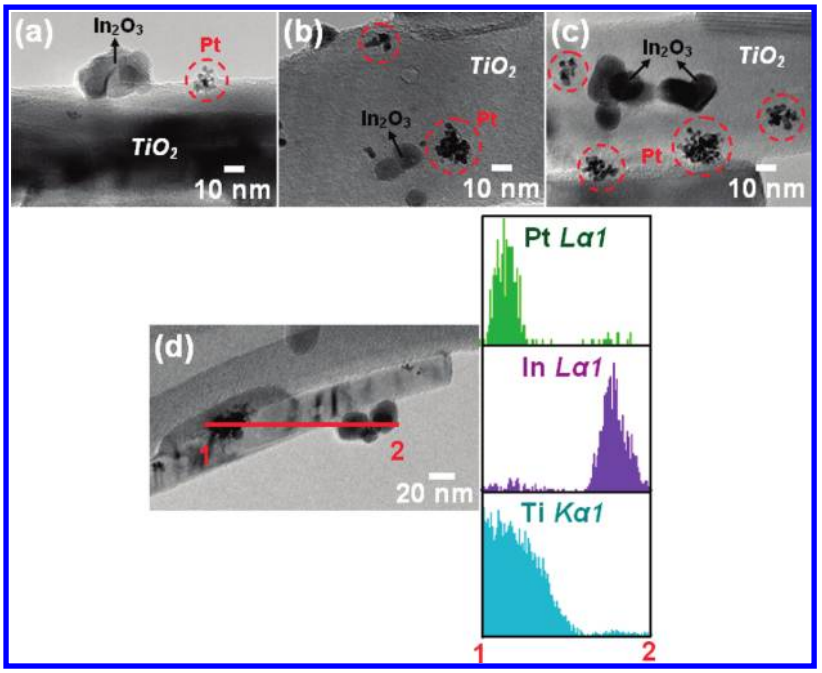

Figure 2. TEM images for In_2O_3–TiO_2–Pt NBs with Pt content of (a) 1.0, (b) 5.0, and (c) 10.0 wt %. Inserted notations indicate the regions of In_2O_3, TiO_2, and Pt compositions for the samples. The corresponding TEM-EDS analysis was shown in (d).

the resultant RhB emission, indicating that the deposited Pt promoted the charge separation for RhB by mediating the interfacial charge transfer of NBs. It might be argued that the direct transfer of photoexcited electrons from RhB to TiO_2 NBs and from RhB to Pt nanoparticles may contribute to the RhB emission depression observed for RhB/In_2O_3–TiO_2 and RhB/In_2O_3–TiO_2–Pt samples. To clarify this issue, RhB, which contained pristine TiO_2 NBs and Pt nanoparticles, respectively, was characterized with PL measurement. The results (data not shown here) show that the emission of RhB in the presence of TiO_2 and Pt was not significantly quenched, suggesting that the electronic interactions of RhB with TiO_2 and Pt were relatively insignificant. This demonstration supports our argument that the more pronounced emission depression of RhB observed for RhB/In_2O_3–TiO_2 and RhB/In_2O_3–TiO_2–Pt samples was mainly a consequence of the further electron transfer from In_2O_3 to TiO_2. To elucidate the effect of Pt deposition on the interfacial charge transfer of In_2O_3–TiO_2 NBs, we compared the photocurrent responses of four relevant sample electrodes by inserting them in a photoelectrochemical cell. Figure 3b depicts the photocurrent generation for pristine TiO_2 NB, pure In_2O_3 nanocrystal, In_2O_3–TiO_2 NB, and In_2O_3–TiO_2–Pt NB electrodes subjected to white light irradiation. We noticed that the In_2O_3–TiO_2 NB electrode yielded greater photocurrents than both pristine TiO_2 NB and pure In_2O_3 nanocrystal electrodes upon light irradiation. The significant charge separation occurring in In_2O_3–TiO_2 NBs may account for such an evident photocurrent enhancement. As noted in the aforementioned section, because of the difference in band structures between In_2O_3 and TiO_2, a pronounced charge separation took place at the In_2O_3/TiO_2 interface of In_2O_3–TiO_2 NBs, resulting in the electron-charged TiO_2 NB body and the hole-enriched In_2O_3 nanocrystal domain. Under this circumstance, the photoexcited electrons would transfer more effectively to FTO substrate via the surface of TiO_2 NBs, while the photogenerated holes at In_2O_3 nanocrystals were captured more readily by the reduced species in electrolyte. Therefore, the photoinduced charge carriers of In_2O_3–TiO_2 NBs were collected more efficiently by the voltameter of the photoelectrochemical cell, which resulted in the generation of higher photocurrents as observed.[18] Upon the deposition of Pt, In_2O_3–TiO_2 NBs exhibited further enhancement in photocurrent generation, manifesting that charge separation of In_2O_3–TiO_2 NBs was significantly improved by introducing Pt. This result is in conformity with our argument that introduction of Pt on TiO_2 surface can mediate the interfacial charge transfer of In_2O_3–TiO_2 NBs to promote the overall charge separation efficiency.

If the observed photocurrent enhancement for In_2O_3–TiO_2 NBs and its dependence on Pt deposition indeed involved electron transfer from In_2O_3 to TiO_2, we should be able to reveal this event in the emission decay profile of the probe molecule RhB. Figure 4a compares the time-resolved PL spectra of RhB under different experimental conditions. The fluorescence of pure RhB in aqueous solution showed monoexponential decay with an emission lifetime of 1.61 ns, close to the reported value of 1.5 ns.[17] The emission decay profiles of RhB in the presence of pure In_2O_3 nanocrystals, In_2O_3–TiO_2 NBs, and In_2O_3–TiO_2–Pt NBs, however, exhibited a biexponential model in which two decay components were derived. The intensity-average lifetime was then calculated to make an overall comparison of the emission decay behavior.[19] The obvious difference in the average emission lifetime of RhB between RhB/In_2O_3 ($\langle\tau\rangle$ = 1.21 ns) and pure RhB ($\langle\tau\rangle$ = 1.61 ns) indicates the emergence of a nonradiative pathway from the electronic interaction between RhB and In_2O_3. This proposition can be confirmed by the emission quenching of RhB observed for RhB/In_2O_3 sample, which further validates the probe role of RhB in this work and its capability of injecting photoexcited electrons into In_2O_3. If electron transfer from RhB to In_2O_3 was the predominant process that dictated the emission quenching of RhB for RhB/In_2O_3 sample, we can estimate the electron-transfer

dx.doi.org/10.1021/jp210033y | J. Phys. Chem. C 2012, 116, 2967–2975

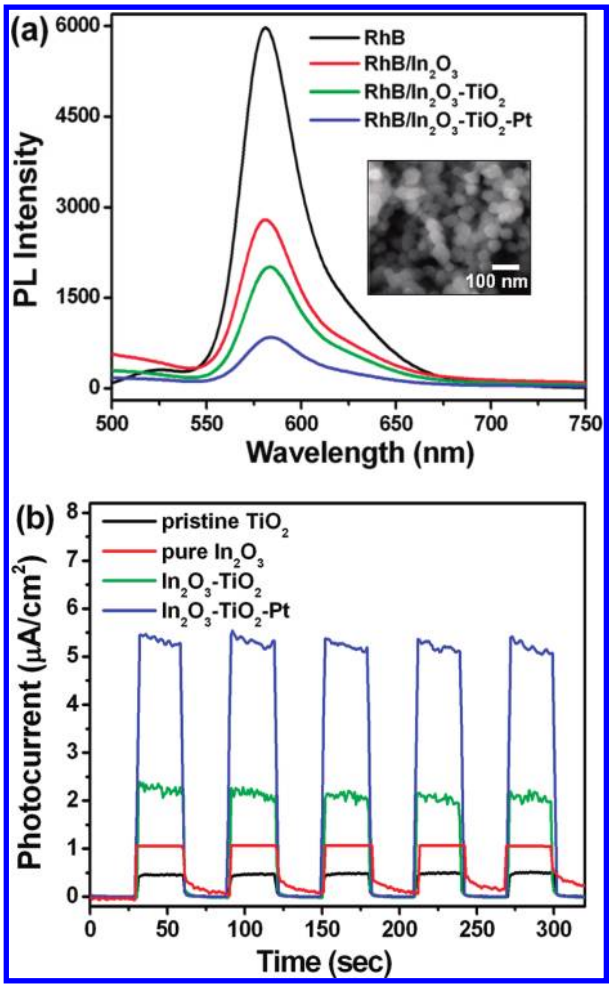

Figure 3. (a) Steady-state PL spectra of RhB in the presence of different samples. The excitation wavelength was 375 nm. Inset shows the SEM image of pure In_2O_3 nanocrystals. (b) Photocurrent responses of different sample electrodes to on/off cycles of light illumination. The content of Pt for In_2O_3–TiO_2–Pt NBs was 1.0 wt %.

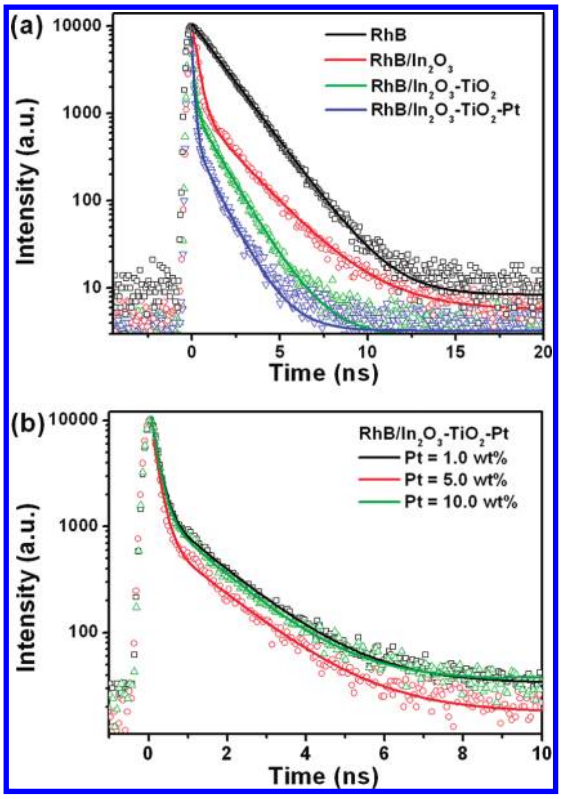

Figure 4. (a) Time-resolved PL spectra of RhB in the presence of different samples. The content of Pt for In_2O_3–TiO_2–Pt NBs was 1.0 wt %. (b) Comparison of PL decay profiles for RhB that contained In_2O_3–TiO_2–Pt NBs with different Pt contents. The fitting results (solid curves) were also included for comparison.

rate constant (k_{et}) by the expression $k_{et}(RhB \rightarrow In_2O_3) = (1/\langle\tau\rangle)(RhB/In_2O_3) - (1/\langle\tau\rangle)(RhB)$, approximately 2.05×10^8 s^{-1}. Table 1 summarizes the electron-transfer rate constants of different processes calculated from relevant samples. It should be noticed that the emission lifetime of RhB in the presence of pristine TiO_2 NBs, and Pt nanoparticles of 1.0, 5.0, and 10.0 wt % was 1.56, 1.59, 1.58, and 1.55 ns, respectively, giving k_{et} (RhB → TiO_2), k_{et} (RhB → Pt-1), k_{et} (RhB → Pt-5), and k_{et} (RhB → Pt-10) as 0.20×10^8, 0.08×10^8, 0.12×10^8, and 0.24×10^8 s^{-1}. These values were about an order of magnitude smaller than that of k_{et} (RhB → In_2O_3), verifying the relatively insignificant electronic interactions of RhB with TiO_2 and Pt. For RhB that contained In_2O_3–TiO_2 NBs, the average emission lifetime ($\langle\tau\rangle$ = 1.05 ns) was found to be shorter than that of RhB/In_2O_3. Given that the electronic interaction between RhB and TiO_2 was relatively minor, we ascribed the RhB emission lifetime shortening of RhB/In_2O_3–TiO_2 to the further electron transfer from In_2O_3 to TiO_2. By comparison of the average lifetime of RhB between RhB/In_2O_3–TiO_2 and RhB/In_2O_3 samples and deducting the contribution of electron transfer from RhB to TiO_2, we obtained k_{et} (In_2O_3 → TiO_2) as 1.06×10^8 s^{-1}. When Pt of 1.0 wt % was present on the TiO_2 surface of In_2O_3–TiO_2 NBs, the shrinkage of RhB emission lifetime became more noticeable ($\langle\tau\rangle$ = 0.86 ns for RhB/In_2O_3–TiO_2–Pt-1), inferring the even further electron transfer from TiO_2 to Pt through the TiO_2/Pt interface upon light irradiation. By use of an analogous calculation method, k_{et} (TiO_2 → Pt-1) was determined to be 2.03×10^8 s^{-1}, almost two times higher than k_{et} (In_2O_3 → TiO_2). This result corroborates that Pt acted as an effective electron-transfer mediator for In_2O_3–TiO_2 NBs by readily accepting photoexcited electrons from TiO_2, which led to the increasingly pronounced charge separation for In_2O_3–TiO_2–Pt NBs as revealed in the depressed RhB emission as well as the enhanced photocurrent generation. To highlight the contribution of Pt to the overall charge separation of NBs, TiO_2 and Pt were regarded as an individual of electron acceptor for In_2O_3, from which the apparent rate constant of electron scavenging from In_2O_3 (k_{es}) can be computed, approximately 3.09×10^8 s^{-1} for In_2O_3–TiO_2–Pt-1 NB sample.

Unlike the system of CdSe-Pt composite micelles where the electron transfer from CdSe to Pt was much faster than the micellar content-exchange and was therefore independent of Pt concentration,[20] Pt in the present In_2O_3–TiO_2–Pt NBs had a quantitative effect since Pt was always existent at TiO_2 surface in the course of carrier transfer. As represented in Figure 4b, when Pt content of In_2O_3–TiO_2–Pt NBs was increased from 1.0 to 5.0 wt %, the emission lifetime of the probe RhB was decreased from 0.86 to 0.68 ns. This phenomenon signifies that Pt of 5.0 wt % mediated the interfacial charge transfer of In_2O_3–TiO_2 NBs more significantly by attracting more electrons from TiO_2, which conduced to the more pronounced charge carrier separation for In_2O_3–TiO_2–Pt-5 sample with an apparent electron-scavenging rate constant of 6.12×10^8 s^{-1}.

dx.doi.org/10.1021/jp210033y | J. Phys. Chem. C 2012, 116, 2967–2975

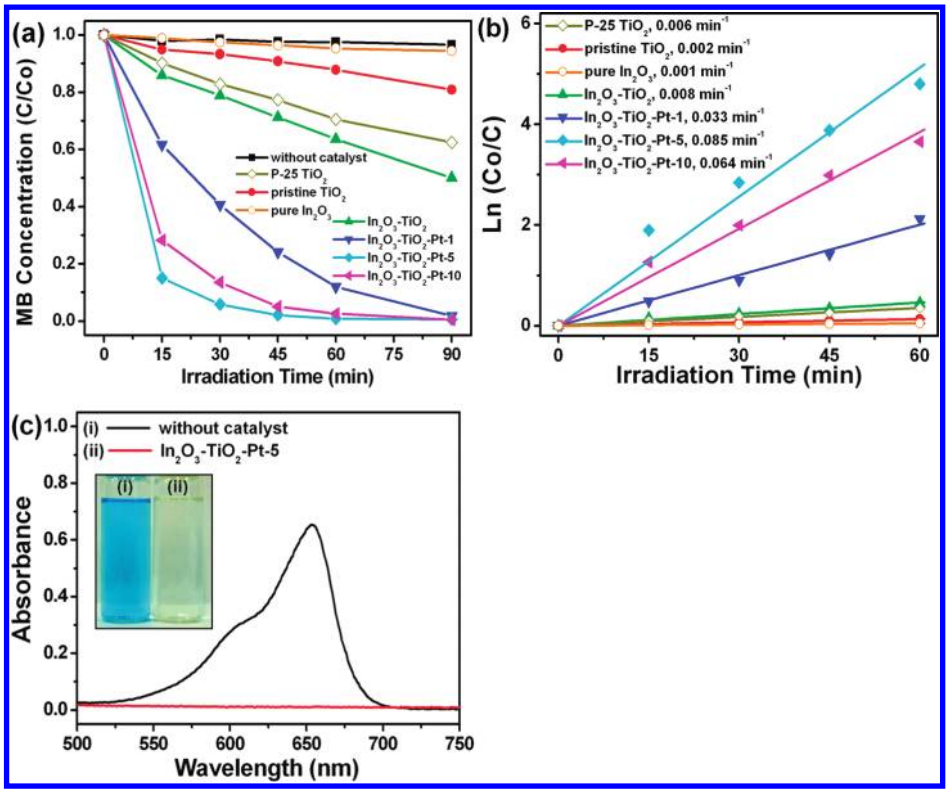

Figure 5. (a) C/C_0 vs irradiation time plots for MB photodegradation under UV illumination without any catalyst and in the presence of seven relevant samples. (b) The corresponding $\ln(C/C_0)$ vs irradiation time plots with the fitting results included. (c) Absorption spectra of MB solutions after exposure of 1 h of daytime sunlight without any catalyst and in the presence of In_2O_3–TiO_2–Pt-5 NBs. Inset shows the corresponding solution color.

Further increase in the content of Pt for In_2O_3–TiO_2–Pt NBs (10.0 wt %), however, caused a lengthened emission lifetime of RhB ($\langle\tau\rangle$ = 0.80 ns), suggesting that charge separation of In_2O_3–TiO_2 NBs turned decreasingly conspicuous as Pt of 10.0 wt % was introduced. The corresponding apparent electron-scavenging rate constant was estimated to be 3.80×10^8 s^{-1}. It is generally believed that, when put in contact with semiconductors, metal with an excess amount has a detrimental influence on the resultant charge separation property.[21] The substantially abundant electrons trapped at excess metal may enable easy encounters with the delocalized holes at semiconductors (i.e., back electron transfer), leading to the depletion of photoinduced charge carriers as well as the suppression in overall charge separation. For the present In_2O_3–TiO_2–Pt NBs, Pt nanoparticles with the content of 10.0 wt % became more of electron–hole recombination centers instead of electron–hole separation enhancers, which alleviated the extent of electron scavenging from In_2O_3 to result in the decreasingly conspicuous charge carrier separation for In_2O_3–TiO_2–Pt-10 sample.

To further examine the fate of photoinduced charge carriers for the present In_2O_3–TiO_2–Pt NBs, a series of photocatalysis experiments were performed in this work. MB, a cationic dye that can be decomposed by accepting electrons following the irradiation on photocatalysts,[22] was used as the test pollutant to monitor the photocatalysis progress for the samples. Seven kinds of photocatalysts including five NB samples (pristine TiO_2, In_2O_3–TiO_2, In_2O_3–TiO_2–Pt-1, In_2O_3–TiO_2–Pt-5, In_2O_3–TiO_2–Pt-10), pure In_2O_3 nanocrystals, and commercial P-25 TiO_2 powder were used for MB photodegradation under the same experimental conditions. The comparative results were shown in Figure 5a, from which several points can be observed. First, experiment in the absence of photocatalyst showed almost no MB photodegradation under UV illumination. Because MB itself was not pyrolyzed in UV light, the vigorous activity of the samples observed here was entirely attributed to the outcome of photocatalysis. Second, In_2O_3–TiO_2 NBs performed better toward MB photodegradation than pristine TiO_2 NBs and pure In_2O_3 nanocrystals, which can be accounted for by the effective charge separation that occurred at the interface of In_2O_3 and TiO_2. This demonstration again addresses the benefit of the binary semiconductor composites for photocatalytic applications.[2,3] Third, the photocatalytic efficiency of In_2O_3–TiO_2 NBs was significantly improved upon the deposition of 1.0 wt % Pt. This improvement mainly emanated from the deposited Pt that can promote the overall charge separation of NBs by readily accepting photoexcited electrons from TiO_2, thereby providing a considerable amount of free electrons for participation in MB degradation. For In_2O_3–TiO_2–Pt NBs with higher Pt content (5.0 wt %), an even better performance in MB photodegradation was attained, probably due to the much more pronounced charge separation of NBs caused by the increasing amount of Pt. Nevertheless, a depressed efficiency of MB photodegradation was observed for In_2O_3–TiO_2–Pt NBs as the content of Pt was further increased to 10.0 wt %. We believed that the substantially abundant electrons trapped at excess Pt would encourage the electron–hole recombination to deplete the photoinduced charge carriers of NBs,[21] thus leading to the depression in the resultant photocatalytic efficiency. In addition, the increase in surface coverage by excess Pt reduced the light absorption of NBs,[23] which also contributed to the decreasing trend of photocatalytic activity observed for In_2O_3–TiO_2–Pt-10 NBs. Furthermore, as compared to the commercial P-25 TiO_2 powder, the three In_2O_3–TiO_2–Pt NB samples all exhibited superior photocatalytic

dx.doi.org/10.1021/jp210033y | J. Phys. Chem. C 2012, 116, 2967–2975

performance under UV illumination, demonstrating their potential as an active photocatalyst in relevant redox reactions. The kinetic curves of MB photodegradation in Figure 5a can be further approximated as a pseudofirst-order process which allowed us to determine the apparent rate constant (k_{MB}) and quantitatively compare the performance of different samples.[24] By use of the fitting results of Figure 5b, we obtained the value of k_{MB} as 0.002, 0.008, 0.033, 0.085, 0.064, 0.001, and 0.006 min^{-1} for pristine TiO_2 NBs, In_2O_3–TiO_2 NBs, In_2O_3–TiO_2–Pt-1 NBs, In_2O_3–TiO_2–Pt-5 NBs, In_2O_3–TiO_2–Pt-10 NBs, pure In_2O_3 nanocrystals, and P-25 TiO_2 powder, respectively. Since In_2O_3 has a direct bandgap of 2.8 eV that corresponds well with the visible light,[10] it may sensitize TiO_2 to enable photocatalysis under visible light illumination. To explore the potential as a reliable visible-light-driven photocatalyst for In_2O_3–TiO_2–Pt NBs, their phtocatalytic performance under natural sunlight was also evaluated. As illustrated in Figure 5c, after exposure to 1 h of daytime sunlight, MB was totally degraded by using In_2O_3–TiO_2–Pt-5 NBs, accompanied by an obvious decoloration of the resultant solution. This result shows that the present In_2O_3–TiO_2–Pt NBs can be used as highly efficient photocatalysts which may practically harvest energy from sunlight.

It is interesting to note that the change in photocatalytic activity with Pt content for In_2O_3–TiO_2–Pt NBs corresponded well with the result of electron-scavenging rate constant variation. This consequence could be realized by the causal relation between charge transfer mediation and free electron extraction. When Pt nanoparticles with a suitable amount (1.0 and 5.0 wt %) were deposited on TiO_2 surface, the interfacial charge transfer of NBs was highly mediated to render the facilitated electron scavenging from In_2O_3, giving rise to an increased amount of photoexcited free electrons that could be extracted for further utilization. The rise in the number of the possibly extracted free electrons for NBs further led to the enhancement in the resultant photocatalytic performance. As Pt content (10.0 wt %) exceeded a critical value, the electron–hole recombination was encouraged in the interior of In_2O_3–TiO_2–Pt NBs, which retarded the electron scavenging from In_2O_3 to impede the free electron extraction. As a result, a depressed photocatalytic activity was observed for In_2O_3–TiO_2–Pt-10 NBs. For more clarity on this relation, we depicted the correlations of electron-scavenging rate constant (k_{es}) and rate constant of MB photodegradation (k_{MB}) with the content of Pt for In_2O_3–TiO_2–Pt NBs in Figure 6.

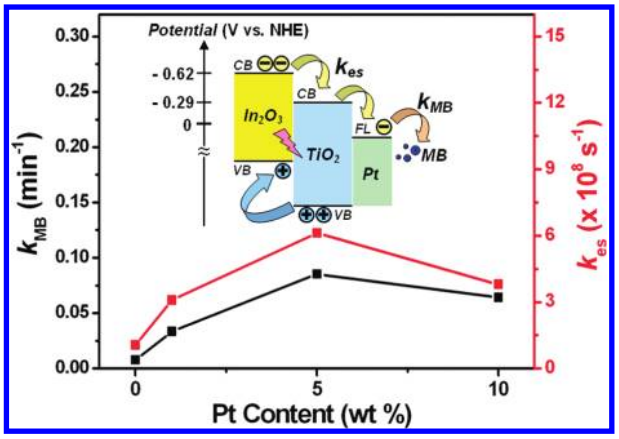

Figure 6. Correlations of electron-scavenging rate constant (k_{es}) and rate constant of MB photodegradation (k_{MB}) with the content of Pt for In_2O_3–TiO_2–Pt NBs.

CONCLUSIONS

In conclusion, the interfacial charge carrier dynamics of three-component In_2O_3–TiO_2–Pt heterojenction system were investigated and presented. With the introduction of Pt on TiO_2 surface, a fluent electron transfer from In_2O_3, through TiO_2, and eventually to Pt was achieved, giving rise to the increasingly pronounced charge separation property for the as-prepared In_2O_3–TiO_2–Pt NBs. The remarkable charge separation of the samples was revealed in the significant enhancement of photocurrent generation. Time-resolved PL data showed that an increased apparent electron-scavenging rate constant was observed for In_2O_3–TiO_2–Pt NBs, attributable to the deposited Pt that can mediate the interfacial charge transfer of NBs to promote the overall charge separation efficiency. On the other hand, the charge carrier transfer in In_2O_3–TiO_2–Pt NBs under light illumination was characterized with a photocatalytic process. The photocatalytic activity of In_2O_3–TiO_2–Pt NBs was fond to surpass those of pristine TiO_2 NBs, pure In_2O_3 nanocrystals, In_2O_3–TiO_2 NBs and commercial P-25 TiO_2 powder, presumably resulting from the more pronounced charge separation property of In_2O_3–TiO_2–Pt heterojunction system. The correlation of photocatalytic activity with the content of Pt for In_2O_3–TiO_2–Pt NBs was in good agreement with that of apparent electron-scavenging rate constant, which can be realized by the direct correspondence between charge transfer mediation and free electron extraction. The present In_2O_3–TiO_2–Pt NBs may find promising photoconversion applications, especially in heterogeneous photocatalysis and photoelectrochemical solar cells. The current work incites one to further explore the coupling of binary semiconductor composites with additional metal by taking into account the suggested origins of the increasingly pronounced charge separation property as guidelines.

AUTHOR INFORMATION

Corresponding Author

*E-mail: yhsu@cc.nctu.edu.tw.

ACKNOWLEDGMENTS

This work was financially supported by the National Science Council of the Republic of China (Taiwan) under Grant No. NSC-100-2113-M-009-004.

REFERENCES

(1) (a) Kamat, P. V. *J. Phys. Chem. C* **2008**, *112*, 18737–18753. (b) Kamat, P. V.; Tvrdy, K.; Baker, D. R.; Radich, J. G. *Chem. Rev.* **2010**, *110*, 6664–6688. (c) Tvrdy, K.; Frantsuzovc, P. A.; Kamat, P. V. *Proc. Natl. Acad. Sci. U. S. A.* **2011**, *108*, 29–34.

(2) (a) Zhang, X.; Zhang, L.; Xie, T.; Wang, D. *J. Phys. Chem. C* **2009**, *113*, 7371–7378. (b) Liu, L.; Hensel, J.; Fitzmorris, R. C.; Li, Y.; Zhang, J. Z. *J. Phys. Chem. Lett.* **2010**, *1*, 155–160. (c) Zhang, J.; Bang, J. H.; Tang, C.; Kamat, P. V. *ACS Nano* **2010**, *4*, 387–395. (d) Bang, J. H.; Kamat, P. V. *Adv. Funct. Mater.* **2010**, *20*, 1970–1976. (e) Zhou, W.; Liu, H.; Wang, J.; Liu, D.; Du, G.; Cui, J. *ACS Appl. Mater. Interfaces* **2010**, *2*, 2385–2392. (f) Wang, H.; Bai, Y.; Zhang, H.; Zhang, Z.; Li, J.; Guo, L. *J. Phys. Chem. C* **2010**, *114*, 16451–16455.

(3) (a) Wang, Z.; Huang, B.; Dai, Y.; Qin, X.; Zhang, X.; Wang, P.; Liu, H.; Yu, J. *J. Phys. Chem. C* **2009**, *113*, 4612–4617. (b) Zhang, Z.; Shao, C.; Li, X.; Zhang, L.; Xue, H.; Wang, C.; Liu, Y. *J. Phys. Chem. C* **2010**, *114*, 7920–7925. (c) Cheng, H.; Huang, B.; Dai, Y.; Qin, X.; Zhang, X. *Langmuir* **2010**, *26*, 6618–6624. (d) Zhang, Y. C.; Du, Z. N.; Li, K. W.; Zhang, M.; Dionysiou, D. D. *ACS Appl. Mater. Interfaces* **2011**, *3*, 1528–1537. (e) Shemesh, Y.; Macdonald, J. E.; Menagen, G.; Banin, U. *Angew. Chem., Int. Ed.* **2011**, *50*, 1185–1189. (f) Cho, S.;

Jang, J. W.; Kim, J.; Lee, J. S.; Choi, W.; Lee, K. H. *Langmuir* **2011**, *27*, 10243−10250.
(4) Kongkanand, A.; Tvrdy, K.; Takechi, K.; Kuno, M.; Kamat, P. V. *J. Am. Chem. Soc.* **2008**, *130*, 4007−4015.
(5) Chakrapani, V.; Tvrdy, K.; Kamat, P. V. *J. Am. Chem. Soc.* **2010**, *132*, 1228−1229.
(6) (a) Reddy, B. M.; Ganesh, I.; Khan, A. *Appl. Catal. A: Gen.* **2003**, *248*, 169−180. (b) Hu, C.; Lan, Y.; Qu, J.; Hu, X.; Wang, A. *J. Phys. Chem. B* **2006**, *110*, 4066−4072. (c) Liu, Y.; Guo, L.; Yan, W.; Liu, H. *J. Power Sources* **2006**, *159*, 1300−1304. (d) Jing, D.; Guo, L. *Catal. Commun.* **2007**, *8*, 795−799. (e) Navarro, R. M.; del Valle, F.; Fierro, J. L. G. *Int. J. Hydrog. Energy* **2008**, *33*, 4265−4273. (f) Stroyuk, A. L.; Kryukov, A. I.; Kuchmii, S. Y.; Pokhodenko, V. D. *Theor. Exp. Chem.* **2009**, *45*, 209−233.
(7) (a) Park, H.; Choi, W.; Hoffmann, M. R. *J. Mater. Chem.* **2008**, *18*, 2379−2385. (b) Jang, J. S.; Choi, S. H.; Kim, H. G.; Lee, J. S. *J. Phys. Chem. C* **2008**, *112*, 17200−17205. (c) Kang, Q.; Lu, Q. Z.; Liu, S. H.; Yang, L. X.; Wen, L. F.; Luo, S. L.; Cai, Q. Y. *Biomaterials* **2010**, *31*, 3317−3326. (d) Daskalaki, V. M.; Antoniadou, M.; Puma, G. L.; Kondarides, D. I.; Lianos, P. *Environ. Sci. Technol.* **2010**, *44*, 7200−7205.
(8) (a) Tada, H.; Mitsui, T.; Kiyonaga, T.; Akita, T.; Tanaka, K. *Nat. Mater.* **2006**, *5*, 782−786. (b) Zhu, H.; Yang, B.; Xu, J.; Fu, Z.; Wen, M.; Guo, T.; Fu, S.; Zuo, J.; Zhang, S. *Appl. Catal. B: Environ.* **2009**, *90*, 463−469. (c) Shen, S.; Guo, L.; Chen, X.; Ren, F.; Kronawitter, C. X.; Mao, S. S. *Int. J. Green Nanotech: Mater. Sci. Eng.* **2010**, *1*, 94−104. (d) Yun, H. J.; Lee, H.; Kim, N. D.; Lee, D. M.; Yu, S.; Yi, J. *ACS Nano* **2011**, *5*, 4084−4090.
(9) (a) Maeda, K.; Domen, K. *J. Phys. Chem. Lett.* **2010**, *1*, 2655−2661. (b) Abe, R. *J. Photochem. Photobiol., C* **2010**, *11*, 179−209.
(10) Xu, Y.; Schoonen, M. A. A. *Am. Mineral.* **2000**, *85*, 543−556.
(11) Pu, Y.-C.; Chen, Y.-C.; Hsu, Y.-J. *Appl. Catal. B: Environ.* **2010**, *97*, 389−397.
(12) (a) Tsai, C.-C.; Teng, H. *Chem. Mater.* **2004**, *16*, 4352−4358. (b) Fu, N.; Wu, Y.; Jin, Z.; Lu, G. *Langmuir* **2010**, *26*, 447−455.
(13) Bedjat, I.; Kamat, P. V. *J. Phys. Chem.* **1995**, *99*, 9182−9188.
(14) Ruankham, P.; Sae-kung, C.; Mangkorntong, N.; Mangkorntong, P.; Choopun, S. *CMU. J. Nat. Sci. Special Issue on Nanotechnology* **2008**, *7*, 177−183.
(15) (a) Basu, B. B. J.; Vasantharajan, N. *J. Lumin.* **2008**, *128*, 1702−1708. (b) Williams, G.; Kamat, P. V. *Langmuir* **2009**, *25*, 13869−13873.
(16) (a) Harada, M.; Einaga, H. *Langmuir* **2006**, *22*, 2371−3277. (b) Harada, M.; Okamoto, K.; Terazima, M. *Langmuir* **2006**, *22*, 9142−9149.
(17) Lei, P.; Chen, C.; Yang, J.; Ma, W.; Zhao, J.; Zang, L. *Environ. Sci. Technol.* **2005**, *39*, 8466−8474.
(18) (a) Zhang, H.; Zong, R.; Zhu, Y. *J. Phys. Chem. C* **2009**, *113*, 4605−4611. (b) Wen, D.; Guo, S.; Wang, Y.; Dong, S. *Langmuir* **2010**, *26*, 11401−11406.
(19) Yang, T.-T.; Chen, W.-T.; Hsu, Y.-J.; Wei, K.-H.; Lin, T.-Y.; Lin, T.-W. *J. Phys. Chem. C* **2010**, *114*, 11414−11420.
(20) Harris, C.; Kamat, P. V. *ACS Nano* **2010**, *4*, 7321−7330.
(21) (a) Lu, W.; Gao, S.; Wang, J. *J. Phys. Chem. C* **2008**, *112*, 16792−16800. (b) Chen, W.-T.; Hsu, Y.-J. *Langmuir* **2010**, *26*, 5918−5925. (c) Mao, A.; Park, N. G.; Han, G. Y.; Park, J. H. *Nanotechnology* **2011**, *22*, 175703−175709.
(22) (a) Kobasa, I. M.; Tarasenko, G. P. *Theor. Exp. Chem.* **2002**, *38*, 255−258. (b) Kobasa, I. M.; Kondrat'eva, I. V.; Gnatyuk, Yu. I. *Theor. Exp. Chem.* **2008**, *44*, 42−47.
(23) (a) Arabatzis, I. M.; Stergiopoulos, T.; Andreeva, D.; Kitova, S.; Neophytides, S. G.; Falaras, P. *J. Catal.* **2003**, *220*, 127−135. (b) Bao, N.; Shen, L.; Takata, T.; Domen, K. *Chem. Mater.* **2008**, *20*, 110−117.
(24) Konstantinou, I. K.; Albanis, T. A. *Appl. Catal. B: Environ.* **2004**, *49*, 1−14.